On the sporadic nature of meridional heat transport by transient eddies

G. Messori and A. Czaja

Space and Atmospheric Physics Group,

Department of Physics, Imperial College London[1]

November 15, 2011

Key words: atmosphere, probability density function, extreme event, Eady waves, baroclinic systems

[1] Author address: G. Messori, Imperial College London, Prince Consort Road, Huxley Building, Room 714; London SW7 2AZ, UK. tel: +44 (0) 20 7594 7773 email: gabriele.messori06@imperial.ac.uk.

Abstract

The present study analyses meridional atmospheric heat transport, due to transient eddies, in the European Centre for Medium-Range Weather Forecasts ERA-Interim reanalysis. Daily, 0.7° latitude and longitude resolution data at the 850mb pressure level is used. Probability density functions (PDFs) of meridional transient eddy heat transport display a near-zero most likely value and a very large skewness, which highlights the dominant role played by extreme events. When considering zonal sections, in both the Northern and Southern Hemispheres, events in the top 5 percentiles typically contribute to over half of the net poleward transport. As a result of this sensitivity to extremes, a large fraction of the heat transport by transient eddies, at a given location and season, is realised through randomly spaced bursts (a few per season), rather than through a continuum of events.

The predominance of extreme events can be explained by the favourable phase relationship between meridional velocity and moist static energy temporal anomalies. This and the spatiotemporal characteristics of the events are compatible with Eady type growing systems.

1. Introduction

Low latitudes experience a net gain of radiative energy, while high latitudes experience a net deficit; as a result of this imbalance, the oceans and the atmosphere transport heat poleward. From the earliest studies of climate dynamics, this transport has been acknowledged as the key to predict the time mean structure of the Earth's climate (e.g. Budyko, 1969; Sellers, 1969; Stone 1978), and its variability (e.g. Bjerknes, 1964). More recent studies have emphasised the role atmospheric heat transport plays in the response of our climate to anthropogenic forcing, especially at high latitudes (e.g. Alexeev *et al.*, 2005; Langen and Alexeev, 2007). For example, there is evidence that anomalies in atmospheric poleward heat transport might explain the 2007 polar sea-ice minimum (Graversen *et al.*, 2011).

The present study focuses on the contribution of time dependent motions to atmospheric poleward heat transport. In mid-to-high latitudes, the latter account for the bulk of the atmospheric heat transport. This is especially true in the Southern Hemisphere (SH), where the contribution of stationary waves is small; in the wintertime Northern Hemisphere (NH) stationary and transient eddies provide comparable transports (Peixoto and Oort, 1992). Wallace and Lau (1979) have produced a comprehensive analysis of meridional transient eddy heat transport in terms of rotational and irrotational, and divergent and non-divergent, components. This topic has also been the focus of many other studies based on observational (e.g. Lau, 1978) and theoretical (e.g. Branscome, 1983) considerations. A new perspective on the subject was introduced by Swanson and Pierrehumbert (1997), who analysed November-March heat flux probability density functions (PDFs) at three locations in the Pacific storm track. At low levels, the top two percentiles of the distribution were found, surprisingly, to account for 20% of the heat transport.

This paper builds on the study by Swanson and Pierrehumbert (1997) by extending their results to the Northern and Southern Hemispheres, and to the cold and warm seasons. After robustly establishing the sensitivity of the heat transport to extremes, we demonstrate its sporadic and irregular temporal distribution by showing that a large contribution to the transport arises from a few isolated bursts every season. The focus will be on low levels, at which the heat transport by transient motions is strongest (Peixoto and Oort, 1992).

The outline of this paper is as follows. Section 2 describes the data used and outlines the methodology. Section 3 looks at the PDFs of the transport and identifies their salient features. Section 4 briefly characterises the extreme events and analyses their geographical distribution. In Section 5, the events are further explored and their dynamics are interpreted as a linear superposition of large numbers of baroclinic waves of different frequencies and wave numbers. Finally, Section 6 will present some discussion and Section 7 conclusions and scope for further research.

2. Data and Methods

The present study utilises ERA-Interim reanalysis data provided by the European Centre for Medium-Range Weather Forecasts (ECMWF) (Simmons *et al.* 2006). Daily outputs (12:00 UTC) are considered over a period spanning from December 1993 to August 2005, thereby providing twelve DJF (December, January and February) and twelve JJA (June, July and August) time series. The latitude and longitude resolution is approximately 0.7°, and the analysis focuses on the 850 mb pressure level.

Transient eddy heat transports are computed as a product of meridional velocity (v) and moist static energy (H, hereafter also referred to as MSE) temporal anomalies. These are defined as departures from the long term, linearly detrended seasonal mean, and are denoted

by a prime. They are computed at every grid point for 172 latitude bands between 30° N and 89° N and 30° S and 89° S. No other time filtering is applied to the data. In the figures described below, H is always given in Kelvin, after division by the specific heat capacity of dry air (taken to be 1005.7 $JK^{-1}kg^{-1}$), and velocity is positive poleward in both hemispheres. The values of v', H' and v'H' are binned and the resulting distribution is normalised, so that one can relate the number of events in each bin to a percentage of the overall events. Taking the product v'H' for all data points and repeating the binning process yields the desired PDFs for transient eddy heat transport. A key element in the analysis of the PDFs is skewness: a measure of the asymmetry of a distribution or, more formally, the distribution's third standardised moment. Note that a skewness of zero does not necessarily imply symmetry about the mean. Another oft-used indicator is the most likely value, which is taken to be the central value of the bin with the highest frequency of events.

3. Transient eddy heat transport PDFs

3.1 General features of the PDFs

To investigate the statistical distribution of transient eddy heat transport, we begin by computing a composite PDF, taking into consideration all available NH latitude bands (30°−89° N) and DJF time series (1993/4−2004/5). This yields a PDF of almost $5x10^7$ data points, which ensures a smooth and representative distribution. The three panels in Figure 1 show the results for v', H' and transport respectively. The key features of the velocity and MSE PDFs are: i) a very low skewness and a near-symmetrical structure, ii) significant positive and negative tails, and iii) a near zero most likely value when compared to the magnitude of the extreme events. The transport PDF, on the opposite, has i) a very high skewness associated with a highly asymmetric distribution and ii) a positive tail which is

significantly more extended than the negative one. The most likely value of the distribution is two orders of magnitude smaller than the extremes, and can therefore be considered near-zero in terms of heat transport.

The symmetry found in velocity and MSE distributions corresponds to comparable realisations of positive and negative anomalies. Since the mean value of the distributions needs, by definition, to be zero, there is no *a priori* reason to expect one of the two tails to have a radically different profile to the other. The large extreme values appear compatible with wintertime perturbations, considering that the vast domain analysed here includes the Pacific and Atlantic storm tracks. The strong asymmetry found in the transport PDF, on the other hand, is related to the imbalance inherent to meridional heat transport, whereby there must be, as emphasized in Section 1, a net transport from low to high latitudes. Hence, some measure of asymmetry in a transport PDF is to be expected. What is not obvious is that the asymmetry should be related to very pronounced extreme events and a near-zero most likely value.

3.2 The role of extreme events in transient eddy heat transport

A visual assessment of the heat transport PDF (Figure 1c) suggests that poleward transport is heavily affected by a small number of very large events. Table I displays the contribution of the top 2%, 5% and 10% of events to i) the overall and to ii) the poleward-only transports. The values displayed are simply i) the percentage contribution of the selected events to the overall integral of the distribution and ii) the percentage contribution of the selected events to the integral of the positive portion of the distribution. It is immediately clear that, regardless of the percentile used to define extreme events, the higher end of the distribution accounts for a disproportionately large portion of the meridional heat transport. As is shown in Table I, events in the top 5 percentiles typically account for over half of the

net transient eddy heat transport, with the exception of SH JJA where the percentage falls just short of the target. The contribution of the top 10 percentiles during NH JJA even exceeds 100%, indicating that the transport due to those events is larger than the overall net transport. Indeed, the percent contributions systematically peak during the summer months in each hemisphere. These features are found to be independent of the fact that a single pressure level is being analysed. Vertical integrals of v'H' over 1000mb – 1mb, not discussed here, show even higher contributions to the net transport from the upper percentiles.

Looking at the numerical values of the full PDF integrals (not shown), the expected seasonal trend emerges, with the net transport peaking during the winter months of each hemisphere. Although the same cycle is found in the extreme event-only integrals, the variability is attenuated. This explains why the percentage contributions actually peak in the summer months, when the transport is at its weakest. The anomalous percentage found for NH JJA is therefore due to the very pronounced seasonal cycle in net NH transient eddy transport, whose magnitude is not as pronounced in the extreme event-only integral.

The amount of heat carried poleward by transient eddies appears to be largely based on very few, very large events. Obviously, the extremely high contributions found could be due to the overall integral of the distribution being close to zero. The poleward-only contributions, however, show that this is not the case: the same 5 percentiles still account for 35% to 40% of the poleward-only transport (see Table I).

It is important to note that the weight of extreme events is very high regardless of latitude. To make this point, Table II displays the contribution of the top 5% of events to overall and poleward-only heat transport at selected latitudes, rather than averaged over an ensemble of latitudes, as was done in Table I. The values found are in line with those shown in Table I and there is no evidence to suggest that the contribution of extreme events is largest at 45° of latitude, where the transient eddy poleward heat transport is almost at its peak (Peixoto and

Oort, 1992). Indeed, the highest contributions are found at other latitudes, where the net transient eddy transport is smaller. As was seen in Table I, there is an anomalous contribution exceeding 100% for NH JJA (in this case at 30° N). Again, this is due to the full integral of that specific PDF having a smaller value than those of the other distributions. In fact, while the net contribution at 30° N exceeds the second highest entry in the table by a factor of two, the corresponding poleward-only contribution is not even 10% larger than the next highest value.

PDFs analogous to those in Figure 1 have been computed for JJAs and for the SH (not shown here). While the magnitude of extreme events and the skewness of the transport PDFs show some seasonality, the key features of the distributions, identified above, are robust features of the data analysed. Distributions for individual latitude bands, individual seasons and different pressure levels were also computed; significant variability in the magnitude of skewness and extreme events was found but, again, the aforementioned features of the PDFs were found to be robust. Regardless of the exact definition of extreme event in terms of percentile and regardless of hemisphere and season, very few events each season therefore seem to account for over half of the poleward heat transport by transient eddies. This, and the near zero most likely value seen in the PDFs, are therefore inherent properties of the transport distribution and need to be satisfactorily explained.

4. Characterising the extreme events in transient eddy heat transport

4.1 Duration and spatial extent

Having ascertained the importance of extreme events in setting the seasonal mean heat transport by transient motions, it is now necessary to relate them to physical processes in the

atmosphere. To do so, we use a measure of temporal and spatial scales, whose principle is schematized in Fig. 2a. To investigate the spatial scales, the v'H' signal on a given day is plotted as a function of longitude over a full latitude circle. Next, extreme events which fulfil given aspect ratio specifications are selected. In particular, the difference between the maximum of an event and the corresponding local minima is required to be larger than the typical magnitude of the near-zero fluctuations in the heat transport distribution. A lower limit of 10^4 $Wmkg^{-1}$ is chosen to represent this constraint. The same value is set as an upper limit for the difference between the two minima of an event. A width (ω) is then measured as the difference in degrees longitude between the points where v'H' reaches half its maximum (dash-dotted line in Fig. 2a)[2]. From this width, a pseudo-wave number κ is computed as:

$$\kappa = \frac{360}{\omega} \tag{1}$$

Conversely, by plotting the v'H' signal at a given geographical co-ordinate over a season and enforcing the same aspect ratio constraints, the measured width at half maximum is interpreted as a pseudo-period τ. Repeating the above processes for all latitudes, longitudes and days allows one to obtain PDFs of κ and τ associated with extreme v'H' events[3].

The definition of extreme event wavelength in the v'H' signal is equivocal, since the pattern is not necessarily sinusoidal, and extracting the "shape" of the extreme event from the background is nigh on impossible. This is why pseudo-wave number κ and corresponding pseudo-period τ are chosen as measures. However, care should be taken when interpreting them: κ and τ are not the wave number and period corresponding to the wavelength of the

[2] Note that the half maximum point is computed relative to the smaller of the two local minima on either side of the local maximum.

[3] Note that cut-off values for duration and spatial extent are enforced to account for the cases where the half-maximum value is smaller than one of the two minima. In the latter scenario, in fact, the width/duration would be measured as extending all the way to the next point where the v'H' signal went below the half maximum value, hence not yielding the actual extreme event width

extreme event. In fact, in a sinusoidal wave, ω would be half of the wavelength; this 1:2 scaling does not translate perfectly to a non-sinusoidal signal but gives a rough idea of the wave number of the extreme events described here. A similar reasoning applies to τ which, in a sinusoidal wave, would be half of the period of a full wavelength. We therefore define the following:

$$K = \frac{\kappa}{2} \text{ and } T = 2 \cdot \tau, \qquad (2)$$

where K and T are, respectively, the wave number and period corresponding to a full wavelength of an extreme event.

Figure 2 shows the probability distribution functions for b) K and c) T for the Northern Hemisphere. The PDFs were computed using all latitude circles between 30° and 89° N and all DJFs and JJAs from December 1993 to August 2005. Events generally have a wave number lying between 2.5 and 7, with a most likely value in the bin covering values between 4 and 4.5. Hence, the distribution in Figure 2b compares favourably with the typical Eady wave number of 6 (Gill, 1982). The result is also in good agreement with Randel and Held (1991) who find that wintertime heat transport by transients, at 700mb and 47°N, is dominated by wave numbers 4-7. As for what concerns duration, Figure 2c suggests that most extreme events have a period of 2 to 7 days, with a most likely value in the bin including timescales between 4 and 5 days. Taking into account the factor of 2, this means that no extreme event persists for longer than 3 days (this will be further illustrated in Figure 6 below).

At 60° latitude, the midpoint of the domain, wave number 4.25 corresponds to a wavelength of roughly 4700 Km. Taking the period to be 4.0×10^5s (approximately 4.5 days), an order of magnitude calculation yields a phase speed of 11.75 ms^{-1}, which is compatible with a baroclinic system. As a point of comparison, Randel and Held (1991), using ECMWF analyses, find phase speeds for 700mb transient eddies to be of order 5-15 ms^{-1}.

The duration, spatial extent and phase speed of extreme events therefore seem to be within the range expected of Eady-type growing systems, as will be further discussed in Section 6. PDFs analogous to those in Fig. 2 were also computed for the SH (not shown here). Although the spatial extent of the events was slightly larger, the above conclusions were found to hold.

4.2 Geographical distribution

In order to identify the locations where the extreme events occur most frequently, we compute next the number of v'H' events per season per data grid box that fall in the top 5 percentiles of the distribution of v'H'. Figure 3 displays the resulting geographical distribution of extreme events. As expected from the dominant contribution of these events to the seasonal mean heat transport, there are similarities with more traditional measures of storm activity (e.g., maps of time mean transient eddy heat flux, or track density of cyclones – see below).

In the DJF season, there is an almost uninterrupted band of very high values spanning the Southern Ocean between 35° S and 55° S. This is coherent with SH storm track maps, such as those by Hoskins and Hodges (2005). A more discontinuous pattern emerges in the NH, where three areas of high activity can be identified. The first spans from the lee of the Rocky Mountains across continental USA and Canada to the Gulf Stream sector of the North Atlantic. A second one is found over the Greenland and Norwegian Seas. The third area roughly corresponds to the Pacific storm track, with a second local maximum over the Bering Strait. The latter feature, as well as that seen off the North-East coast of Greenland, is distinct from the patterns seen in more traditional storm track diagnostics (e.g. Blackmon, 1976). Since the Bering Strait is at the boundary between cold, dry polar air masses and warmer, moist maritime ones, outflows of cold air over the ocean could explain the local maximum

(e.g. Businger, 1987; Overland and Stabeno, 2004). The very high values found off the North-Eastern coast of Greenland, on the other hand, could be related to mesocyclone genesis occurring in the area (Hoskins and Hodges, 2002).

In the JJA season, the picture in the SH remains similar, although the high activity band is shifted poleward, with a well defined maximum over the Ross Sea. In the NH, the main change is that a high activity area appears over the Barents, Kara and Laptev Seas and over parts of Northern Siberia. A weakening of the Greenland and Gulf Stream maxima and the disappearance of the Bering Strait one are also witnessed.

The poleward shift of events during the JJA season could be explained by the seasonal shifts in the Jet Stream's position. The white contours overlaid onto the colour map in Figure 3 show mean zonal wind speeds at 300 mb. In the DJF season there is good correspondence between areas of high zonal winds and the Gulf Stream and Pacific maxima. There is also agreement in the SH. During the JJA season, two local wind speed maxima appear in correspondence with the Siberian frequency maximum, and there is very good agreement over the Pacific, Gulf Stream and Ross Sea areas.

5. Extreme events in transient eddy heat transport: a wave perspective

As highlighted in Table I, extreme events in the v'H' distribution are key contributors to the net poleward heat transport by transient eddies. To identify the origin of these events, it is useful to picture the v' and H' signals as travelling waves, and to reason in terms of phase relationship and magnitude. An anomalously large v'H' event might occur as a result of:

i) Extremely large velocity and MSE anomalies which, regardless of their phase relationship, yield a very large transport value (magnitude-driven transport).

ii) Non-extreme v’ and H’ events which occur perfectly in phase (phase-driven transport).

Both mechanisms are possible candidates, since the product of peak v’ and H’ values yields transport values which are almost a factor of two greater than the largest events in the v’H’ distribution (see, for example, the values in Figure 1). Obviously, a combination of the two, such as near in-phase, large v’ and H’ events, is entirely possible.

To investigate the phase relationship, a valuable tool is a scatter plot of v’ versus H’. To obtain a clear picture, it is useful to remove all velocity and MSE anomaly data points which do not correspond to extreme v’H’ events. Note that this does not equate to removing all v’ and H’ data points which are not in the top percentiles of velocity and MSE anomaly distributions, as the selection is performed purely in terms of v’H’ percentiles. One can then bin the data points in the scatter plot along the two axes, analogously to a bivariate PDF. Colour coding the resulting distribution yields a discrete colour map, shown in Figure 4. In the latter, the top two quadrants show the results averaging over the latitude band 30°−89° N in JJA and DJF, while the bottom two show the plots for 30°−89° S in the same seasons. The continuous lines in each quadrant show the values of the 5^{th} and 95^{th} percentiles of v’ and H’. The squares labelled S contain all extreme v’H’ occurrences where neither v’ nor H’ are in the top/ bottom five percentiles of their respective distributions.

The most striking feature of the map is the lack of near-zero v’ and H’ data points even though, according to Figure 1, near-zero values are the most likely realisations of the two variables. In a magnitude-dominated scene, extreme events in heat transport would mostly be due to the sheer magnitude of either v’ or H’, regardless of their phase relationship. This would imply the presence of events where one of the two anomalies is small while the other one is extremely large. Such events are not seen in any of the panels in Figure 4. The figure therefore immediately excludes the magnitude-driven transport picture. At the same time, a

large number of the v'H' events are seen to correspond to at least one of the two variables being in the top 5 percentiles of its distribution. In the figure, this corresponds to all data points not within the squares labelled S. Most extreme transport events therefore seem to be due to (near) in-phase velocity and MSE anomalies where at least one of the two variables qualifies as an extreme event. To put a number on this statement, it is found that only 6% to 11% of the v'H' extreme events correspond to both velocity and MSE anomalies which are not in the top 5 percentiles of their respective distributions.

Further proof of the in-phase view can be obtained by normalising velocity and MSE anomalies by their respective standard deviations. Covariance and correlation are related by the following expression:

$$cov(x,y) = corr(x,y)\sigma_x\sigma_y\,, \tag{3}$$

where the correlation component is a measure of phase and the standard deviation one a measure of magnitude. If one normalises both anomalies by their respective standard deviations, and then computes the v'H' PDF as in Figure 1c, only the phase information will be conserved. The results (not presented here) still show large skewness, even though it is smaller than that of their un-normalised counterparts. This confirms that the phase relationship between v' and H' is the key mechanism for generating extreme transport events.

A natural test of the wave picture adopted so far is to consider simple sinusoidal curves for v' and H'. When the latter are in quadrature, for a single amplitude and frequency, the PDF of their product is symmetric about its median value. As can be easily verified, the minimum of the distribution is then found at the median, the most likely value coincides with the two extreme values, and the skewness is null. When the same waves are in phase, the PDF simply shifts towards positive values of v'H', with one of the two most likely values now being at zero, but the shape of the distribution remains unchanged. The latter is therefore far from resembling that shown in Figure 1c.

Next, consider v' and H' being represented by a superposition of sine waves over a broad spectrum of frequencies and amplitudes. The product of a high (say for v') and a low frequency (say for H') wave yields a wave packet-like pattern, with frequent oscillations around zero (not shown). Hence, this interaction is able to reproduce the near-zero most likely value of the v'H' distribution shown in Figure 1c. The extended positive tail of the PDF, on the other hand, originates from the range of amplitudes considered. As discussed above, the product of two sinusoidal curves will yield most likely values at the two extremes of the distribution. For near in-phase waves, such a distribution will mostly cover positive values, and the magnitude of extremes will depend on the amplitude of the two waves. The effect of having a distribution of random amplitudes for near in-phase waves is, therefore, to spread out these most likely values. Those corresponding to the maxima of the distributions will yield a long positive tail. The result is a PDF with a near-zero most likely value and a long positive tail, analogously to that shown in Figure 1c (a simple example is given in Figure 5). This reinforces our interpretation of the distribution of v', H' and their product as resulting from a broad spectrum of travelling baroclinic waves.

6. Discussion

The results found in this study are compatible with the traditional picture of growing systems having the minimal phase shift between v' and H', and accounting for the bulk of the heat transport (Eady, 1949). What is unexpected is that the majority of the transport is carried out by only a few such occurrences every season, in easily identifiable bursts. This can be clearly seen in Figure 6 which illustrates, in a binary format, the sporadic nature of the heat transport process at a single point (60°N 0°E)[4]. On a given day, a value of unity (vertical bar)

[4] Similar plots are obtained for other grid points (not shown).

is set to the curve if v'H' falls in the top 5 percentiles of the distribution for the 60° N latitude circle, and a value of zero is used otherwise (no vertical bars). By definition, there are only a few extreme events every season, yet these account for a very large portion of the overall poleward heat transport at this location, sometimes exceeding 60% (the numbers for each winter are indicated in the top right corner of each panel)! Repeating this analysis for the number of extreme events per day along a full latitude circle (not shown here) yields a similar picture, with bursts of extreme events lasting for a few days and typically involving less than 15 % of the gridpoints at that latitude. This further illustrates the sensitivity of the atmosphere to very few, temporally and spatially localised features.

In their study of the North Pacific storm track, Swanson and Pierrehumbert (1997) noted this large sensitivity to extreme events and were able to reproduce the salient features of the PDF discussed here using a model in which temperature anomalies (akin to H' here) were created by anomalous meridional advection v' and damped through heat exchange with the underlying ocean. This picture is somewhat different from the "wave view" introduced in Section 5, in that they treated temperature as a passive scalar, rather than as coupled to the velocity field like in a growing Eady wave. In addition, Swanson and Pierrehumbert (1997) provided a mechanism limiting the temperature variance (thermal damping), while the mechanisms leading to the equilibrium distribution of baroclinic waves were not addressed in Section 5. Nevertheless, and more importantly, the simplicity of both views suggests that i) one should not be surprised by the large influence of extreme events on the mean poleward heat transport by transient eddies and ii) one should expect to see this statistical signature in very idealized models of the atmosphere and not solely in nature.

To test the latter prediction, we have applied the analysis above to the output of a coupled ocean atmosphere model (FORTE, see Sinha and Smith, 2002 and Smith and Gregory, 2009)

run in an aquaplanet geometry (water covered world, as described in Smith *et al.*, 2006) [5]. In such geometry, the statistics are only functions of latitude and height, and the circulation is dominated by large scale waves developing on the midlatitude westerlies. The results of the PDF analysis at 850mb for FORTE (not shown) were found to be essentially the same as for the ERA-Interim data. This confirms that the sporadic nature of the heat transport, emphasized in our study, has nothing to do with detailed features of the atmosphere's lower boundary (coastline, ocean fronts, sea ice, orography etc.), stationary waves and mesoscale features (excluded by the coarse resolution of FORTE but present in the reanalysis through data assimilation). Rather, this must be an intrinsic property of baroclinic waves in the atmosphere.

7. Conclusions

This paper studies meridional atmospheric heat transport due to transient eddies, focussing on low levels in the mid-latitudes. The analysis is in terms of the probability distribution functions of meridional velocity anomaly v', moist static energy anomaly H' and their product v'H'. Two outstanding features of the distribution of v'H' are the near-zero most likely value and the very pronounced positive skewness. These appear to be robust features of the distribution and are only marginally affected by season, hemisphere or latitude. Outputs from an intermediate complexity climate model, run in an aquaplanet configuration, present similar characteristics. This suggests that the shape of the v'H' PDFs is not due to mesoscale phenomena, stationary waves and complexities associated with surface boundary conditions.

[5] The only difference between the simulation analysed here and that described in Smith et al. (2006) is the increased spatial resolution (T42 rather than T21) and the degraded vertical resolution (15 levels rather than 21).

As a direct consequence of the distribution's skewness, the top 5% of v'H' events accounts for over half of the net poleward heat transport by transient eddies. This large sensitivity to extremes was noted by Swanson and Pierrehumbert (1997) at three locations in the Northwest Pacific during winter. Here, it is being established robustly for all extra-tropical regions as well as winter and summer seasons. It is suggested that the extreme events result from a near in-phase relationship between v' and H' anomalies of sizeable amplitude, as is typically expected from growing Eady waves. Indeed, further analysis shows that extreme events in heat transport have wave numbers and timescales compatible with Eady-type systems. Accordingly, regions where extreme events occur most frequently tend to coincide with the "storm track" regions singled out in previous studies via Eady growth rate diagnostics (e.g. Hoskins and Valdes, 1990), or tracking algorithms (e.g. Hoskins and Hodges, 2002 and Hoskins and Hodges, 2005).

An important consequence of the sensitivity of the heat transport to extreme events is that a very large fraction of the transport occurs in a few discrete bursts, each lasting for only a couple of days. The transient heat transport process in mid-latitudes is therefore fundamentally sporadic in the temporal domain.

This new perspective on mid-latitude heat transport warrants further analysis of the mechanisms controlling the occurrences of extreme events. For example, a stimulating hypothesis is that ocean-atmosphere interactions at the western boundary of ocean basins are instrumental in triggering extremes by setting regions of low atmospheric static stability (as a result of convective events), and hence favouring more Eady growth (Czaja and Blunt, 2011).

The new perspective also has an intriguing application to the climate change debate. Polar amplification has traditionally been ascribed to surface-albedo feedback (e.g. Hall, 2004), but a number of studies have also highlighted the important contribution of atmospheric heat transport to the phenomenon (e.g. Alexeev *et al.*, 2005; Graversen, 2006; Lee *et al.*, 2011).

This suggests that there could be a strong link between extreme transport events and the climate of the Arctic.

The fact that the dominance of extremes in the transient eddy heat transport is present throughout the summer months, which form a consistent part of the polar cap's melt season, also suggests a connection to sea-ice coverage. While it is beyond the scope of this paper, an analysis relating extreme heat transport events to summertime NH sea-ice extent, along the lines of that performed by Graversen *et al.* (2011, hereafter G11), might uncover interesting connections. G11 suggest that the 2007 sea-ice minimum in the Arctic could be linked to atmospheric heat transport. In particular, the study finds anomalous atmospheric poleward heat transport and anomalous atmospheric transport convergence during that year in the region interested by the greatest areal loss of sea-ice. G11 then conclude that the additional downwelling long-wave radiation forcing generated by these atmospheric features had a significant role in initiating the melt process. A natural extension of this work would involve looking for anomalies in the frequency of extreme meridional transient eddy heat transport events in areas of the Arctic subject to enhanced sea-ice melting. Analysing in detail the area of high extreme event frequency found in JJA over part of the Arctic Ocean would offer the perfect starting point. Ultimately, very few days every season could hold the key to explaining some large scale features of our climate system.

Acknowledgements: G. Messori is funded by a bursary from the Natural Environment Research Council. ERA-Interim reanalysis data were obtained from the BADC FTP server at ftp.badc.rl.ac.uk. We thank the anonymous reviewers for the helpful comments. We are also grateful to J. Cheung for providing the FORTE data. A discussion with Prof. S. Minobe helped in structuring the analysis presented in this paper.

References

Alexeev VA, Langen PL, Bates JR. 2005. Polar amplification of surface warming on an aquaplanet in “ghost forcing” experiments without sea ice feedbacks. *Clim. Dyn.* 24: 655-666. DOI: 10.1007/s00382-005-0018-3

Blackmon, ML. 1976. A Climatological Spectral Study of the 500 mb Geopotential Height of the Northern Hemisphere. J. Atmos. Sci. 33: 1607-1623. DOI: 10.1175/1520-0469(1976)033<1607:ACSSOT>2.0.CO;2

Bjerknes J. 1964. Atlantic Air-Sea Interaction. *Adv. Geophys.* 10: 1-82. DOI:10.1016/S0065-2687(08)60005-9

Branscome LE. 1983. A parametrisation of Transient Eddy Heat Flux on a Beta-Plane. *J. Atmos. Sci.* 40: 2508-2521. DOI: 10.1175/1520-0469(1983)040<2508:APOTEH>2.0.CO;2

Budyko MI. 1969. The effect of solar radiation variations on the climate of the Earth. *Tellus* 21: 611-619.

Businger S. 1987. The synoptic climatology of polar-low outbreaks over the Gulf of Alaska and the Bering Sea. *Tellus* 39A: 307-325. DOI: 10.1111/j.1600-0870.1987.tb00310.x

Czaja A, Blunt N. 2011. A new mechanism for ocean–atmosphere coupling in midlatitudes. *Q. J. R. Meteorol. Soc.* 137: 1095-1101. DOI: 10.1002/qj.814

Eady ET. 1949. Long waves and cyclone waves. *Tellus* 1: 33-52.

Gill AE. 1982. *Atmosphere-Ocean Dynamics*. Academic Press: New York; pp. 549 – 560.

Graversen RG. 2006. Do Changes in the Midlatitude Circulation Have Any Impact on the Arctic Surface Air Temperature Trend? *J. Climate* 19: 5422-5438. DOI: 10.1175/JCLI3906.1

Graversen RG, Mauritsen T, Drijfhout S, Tjernström M, Mårtensson S. 2011. Warm winds from the Pacific caused extensive Arctic sea-ice melt in summer 2007. *Clim. Dyn.* 36: 2103-2112. DOI: 10.1007/s00382-010-0809-z

Hall A. 2004. The role of surface albedo feedback in climate. *J. Climate* 17: 1550-1568. DOI: 10.1175/1520-0442(2004)017<1550:TROSAF>2.0.CO;2

Hoskins BJ, Valdes PJ. 1990. On the existence of storm-tracks. *J. Atmos. Sci.* 47: 1854-1864. DOI: 10.1175/1520-0469(1990)047<1854:OTEOST>2.0.CO;2

Hoskins BJ, Hodges KI. 2002. New Perspectives on the Northern Hemisphere Winter Storm Tracks. *J. Atmos. Sci.* 59: 1041-1061. DOI: 10.1016/j.jcis.2005.03.065

Hoskins BJ, Hodges KI. 2005. A New Perspective on Southern Hemisphere Storm Tracks. *J. Climate* 18: 4108–4129. DOI: 10.1175/JCLI3570.1

Langen PL, Alexeev VA. 2007. Polar amplification as a preferred response in an idealized aquaplanet GCM. *Clim. Dyn.* 29: 305-317. DOI: 10.1007/s00382-006-0221-x

Lau NC. 1978. On the Three-Dimensional Structure of the Observed Transient Eddy Statistics of the Northern Hemisphere Wintertime Circulation. *J. Atmos. Sci.* 35: 1900-1923. DOI: 10.1175/1520-0469(1978)035

Lau NC, Wallace JM. 1979. On the Distribution of Horizontal Transports by Transient Eddies in the Northern Hemisphere Wintertime Circulation. *J. Atmos. Sci.* 36: 1844-1861. DOI: 0022-4928/79/101844-18

Lee S, Gong T, Johnson N, Feldstein SB, Pollard D. 2011. On the Possible Link between Tropical Convection and the Northern Hemisphere Arctic Surface Air Temperature Change between 1958 and 2001. *J. Climate* 24: 4350–4367. DOI: 10.1175/2011JCLI4003.1

Overland JE, Stabeno PJ. 2004. Is the Climate of the Bering Sea Warming and Affecting the Ecosystem? *EOS Trans. Am. Geophys. Union* 85: 309-312. DOI: 10.1029/2004EO330001

Peixoto JP, Oort AH. 1992. *Physics of Climate*. American Institute of Physics: New York; pp. 317-336.

Randel WJ, Held IM. 1991. Phase speed spectra of transient eddy fluxes and critical layer absorption. *J. Atmos. Sci.* 48: 688-697. DOI: 10.1175/1520-0469(1991)048<0688:PSSOTE>2.0.CO;2

Sellers WD. A Global Climatic Model Based on the Energy Balance of the Earth-Atmosphere System. *J. Appl. Meteorol.*8: 392-400. DOI: 10.1175/1520-0450(1969)008<0392:AGCMBO>2.0.CO;2

Simmons A, Uppala S, Dee D, Kobayashi S. 2006. ERA-Interim: New ECMWF reanalysis products from 1989 onwards. *ECMWF Newsletter* 110: 25-35

Sinha B, Smith RS 2002. *'Development of a fast coupled general circulation model (FORTE) for climate studies, implemented using the OASIS couple'*. Technical Report 81, 67pp. Southampton Oceanography Centre: Southampton, UK.

Smith RS, Dubois C, Marotzke J. 2006. Global climate and ocean circulation on an aquaplanet ocean-atmosphere general circulation model. *J. Climate* 19: 4719-4737. DOI: 10.1175/JCLI3874.1

Smith RS, Gregory JM. 2009. A study of the sensitivity of ocean overturning circulation and climate to freshwater input in different regions of the North Atlantic. *Geophys. Res. Lett.* 36. DOI: 10.1029/2009GL038607

Stone PH. 1978. Constraints on Dynamical Transports of Energy on a Spherical Planet. *Dyn. Atmos. Oceans* 2: 128-139. DOI: 10.1016/0377-0265(78)90006-4

Swanson K, Pierrehumbert RT. 1997. Lower-Tropospheric Heat Transport in the Pacific Storm Track. *J. Atmos. Sci.* 54: 1533–1543. DOI: 10.1175/1520-0469(1997)054

List of Tables

Contribution of extreme events to meridional transient eddy heat transport for 30°–89° N and 30°–89° S

a) Hemisphere	Percentile	Overall % Weight	Poleward only % weight
N	2	32.1	20.6
	5	58.9	37.7
	10	88.2	56.5
S	2	31.1	22.0
	5	56.9	40.2
	10	84.0	59.4

b) Hemisphere	Percentile	Overall % Weight	Poleward only % weight
N	2	37.3	20.6
	5	69.8	38.5
	10	105.3	58.1
S	2	23.9	18.4
	5	45.3	35.0
	10	69.4	53.6

Table I: Percent contribution of extreme v'H' events in a) DJF and b) JJA to net and poleward only meridional atmospheric heat transport due to transient eddies. The data covers all longitudes and latitudes, from 30°N to 89°N and from 30°S to 89°S, over the twelve seasons considered (December 1993 – August 2005). The percentile column indicates which percentiles of v'H' events are classed as extreme.

Contribution of extreme events to meridional transient eddy heat transport for 30°, 45°, 60° and 75°N and 30°, 45°, 60° and 75° S

a) Hemisphere	Latitude	Overall % Weight	Poleward only % weight
N	30	46.9	36.6
	45	46.6	37.0
	60	58.0	36.3
	75	67.6	38.3
S	30	57.5	39.6
	45	39.5	29.9
	60	44.2	35.0
	75	68.0	43.4

b) Hemisphere	Latitude	Overall % Weight	Poleward only % weight
N	30	120.0	46.2
	45	67.0	38.4
	60	61.3	35.8
	75	54.4	34.5
S	30	39.0	32. 3
	45	33.6	28.6
	60	36.8	30.5
	75	48.4	35.9

Table II: Percent contribution of the top 5 percentiles of v'H' events in a) DJF and b) JJA to net and poleward only meridional atmospheric heat transport due to transient eddies. The data covers latitude circles at 30°, 45°, 60° and 75° N and 30°, 45°, 60° and 75° S over the twelve seasons considered (December 1993 – August 2005).

List of Figures

Figure 1: PDFs of a) meridional velocity anomalies, b) moist static energy anomalies and c) atmospheric heat transport due to transient eddies. The data covers Northern Hemisphere DJFs from December 1993 to February 2005. All latitude circles between 30° and 89° N are taken into account. The skewnesses of the PDFs are respectively a) 0.24, b) 0.02 and c) 2.00. The corresponding most likely values are a) 0.17 ms^{-1}, b) -0.04 K and c) $-7.6x10^{3}$ $Wmkg^{-1}$. The vertical lines show the bins corresponding to the most likely values.

Figure 2: a) Schematic of how the full width/duration at half maximum of the v'H' signal is computed. The three arrows indicate the local maximum corresponding to an extreme event and the two local minima on either side. The double arrow indicates the height of the extreme event relative to the smaller of the two minima. The dash-dot line indicates the measured half-maximum width/duration (ω/τ). In this case, the peak is well defined relative to the local minima and the two minima are close to one another, meaning that the event passes all the aspect ratio tests (see text for details). The two bottom panels are PDFs of b) the wave number K and c) the full duration at half maximum T of extreme v'H' events. The latter are defined as events in the top 5 percentiles of the v'H' distribution. The data range is the same as in Figure 1. The vertical lines show the bins corresponding to the most likely values.

Figure 3: Map of v'H' events in the top 5 percentiles of the v'H' distribution for a) DJF and b) JJA. All twenty-four seasons (December 1993 – August 2005) are taken into consideration. The scale of the colour bar corresponds to the number of data points per season per 0.7° x 0.7° box. The calculation is not applied equatorward of 30° latitude. The white lines are regularly spaced 5 ms^{-1} contours of 300 mb time-averaged zonal winds. The contours range from 0 to 25 ms^{-1}, with positive wind speeds being eastbound.

Figure 4: Colour map of v' and H' data points corresponding to the top 5 percentiles of v'H' events for a) NH JJA, b) NH DJF, c) SH JJA and d) SH DJF. All twenty-four seasons (December 1993 – August 2005) are taken into consideration. The scale of the colour bar corresponds to the number of data points per discrete bin. The continuous lines correspond to the values of the 5^{th} and 95^{th} percentiles of the v' and H' distributions. The squares labelled S contain all extreme v'H' occurrences where neither v' nor H' are in the top/ bottom five percentiles of their respective distributions.

Figure 5: PDF resulting from the product of two linear sums of sinusoidal waves, taken as simple models for v' and H'. The following equations were adopted:

$$v' = \Sigma_i A_i \sin(ix + \varphi_i);\ H' = \Sigma_i B_i \sin(ix + \varphi_i + \Delta\varphi);$$
$$v'H' = \Sigma_i \Sigma_j A_i B_j \sin(ix + \varphi_i)\sin(jx + \varphi_j + \Delta\varphi).$$

Here i and j represent summation over a range of frequencies (corresponding to periods ranging from seasonal to daily scales), each with corresponding amplitudes A_i and B_j and random phases φ_i and φ_j. $\Delta\varphi$ is a fixed phase relationship between all v' and H' waves, here set to $\pi/10$ as an indicative near in-phase scenario. The distribution reproduces both the long positive tail and the near zero most likely value of the v'H' PDF seen in Figure 1c.

Figure 6: Bar plot of v'H' extreme events at 60°N 0°E. Extreme events are defined as events in the top 5 percentiles of the v'H' distribution for the 60°N latitude circle. The twelve panels correspond to DJF seasons from DJF 1993/4 to DJF 2004/5. Bars correspond to an extreme event occurring on a given day; the abscissa indicates the day of the season. The percentages in each panel indicate the contribution of the selected events to the net seasonal meridional transient eddy heat transport. See text for further details.

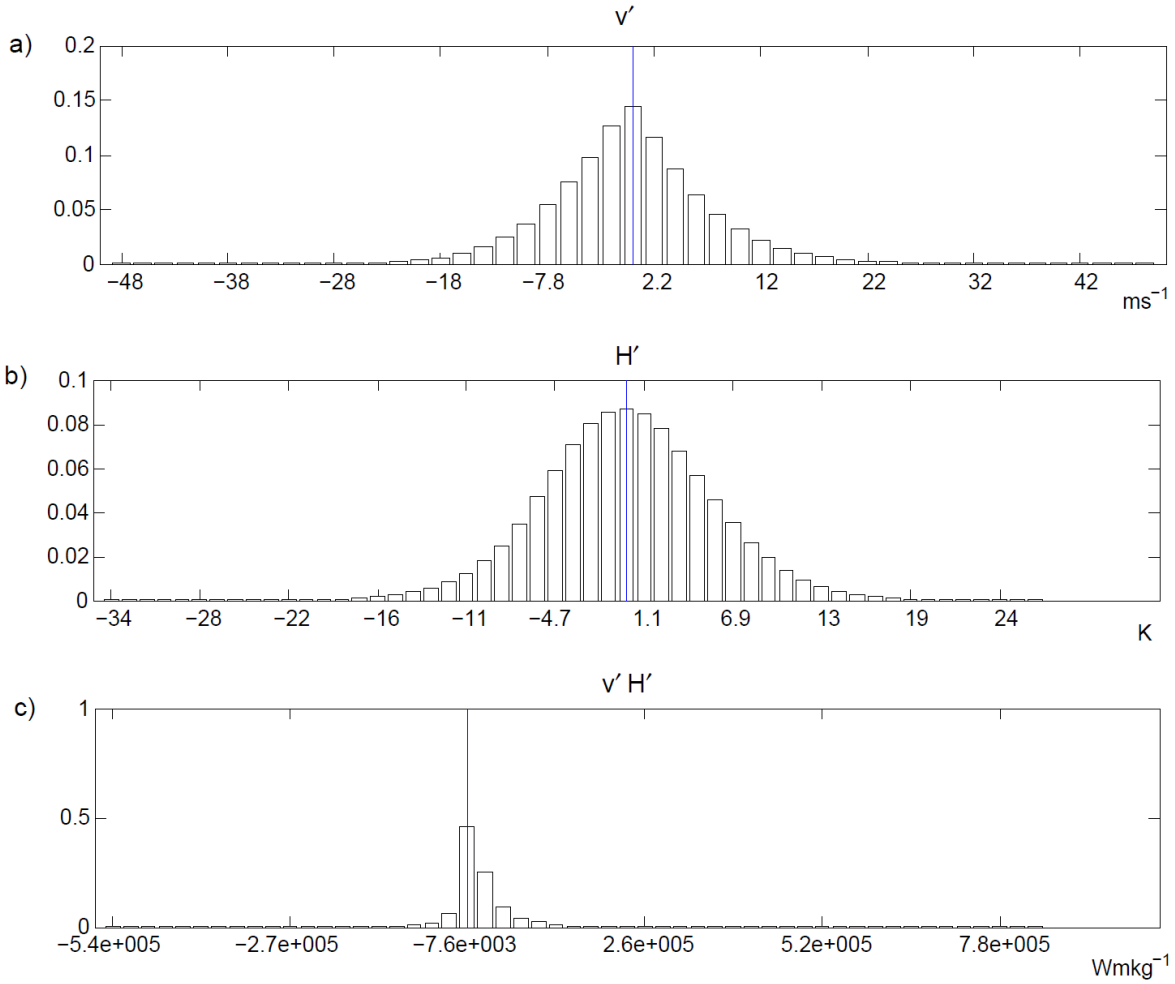

Figure 1: PDFs of a) meridional velocity anomalies, b) moist static energy anomalies and c) atmospheric heat transport due to transient eddies. The data covers Northern Hemisphere DJFs from December 1993 to February 2005. All latitude circles between 30° and 89° N are taken into account. The skewnesses of the PDFs are respectively a) 0.24, b) 0.02 and c) 2.00. The corresponding most likely values are a) 0.17 ms^{-1}, b) -0.04 K and c) -7.6×10^3 $Wmkg^{-1}$. The vertical lines show the bins corresponding to the most likely values.

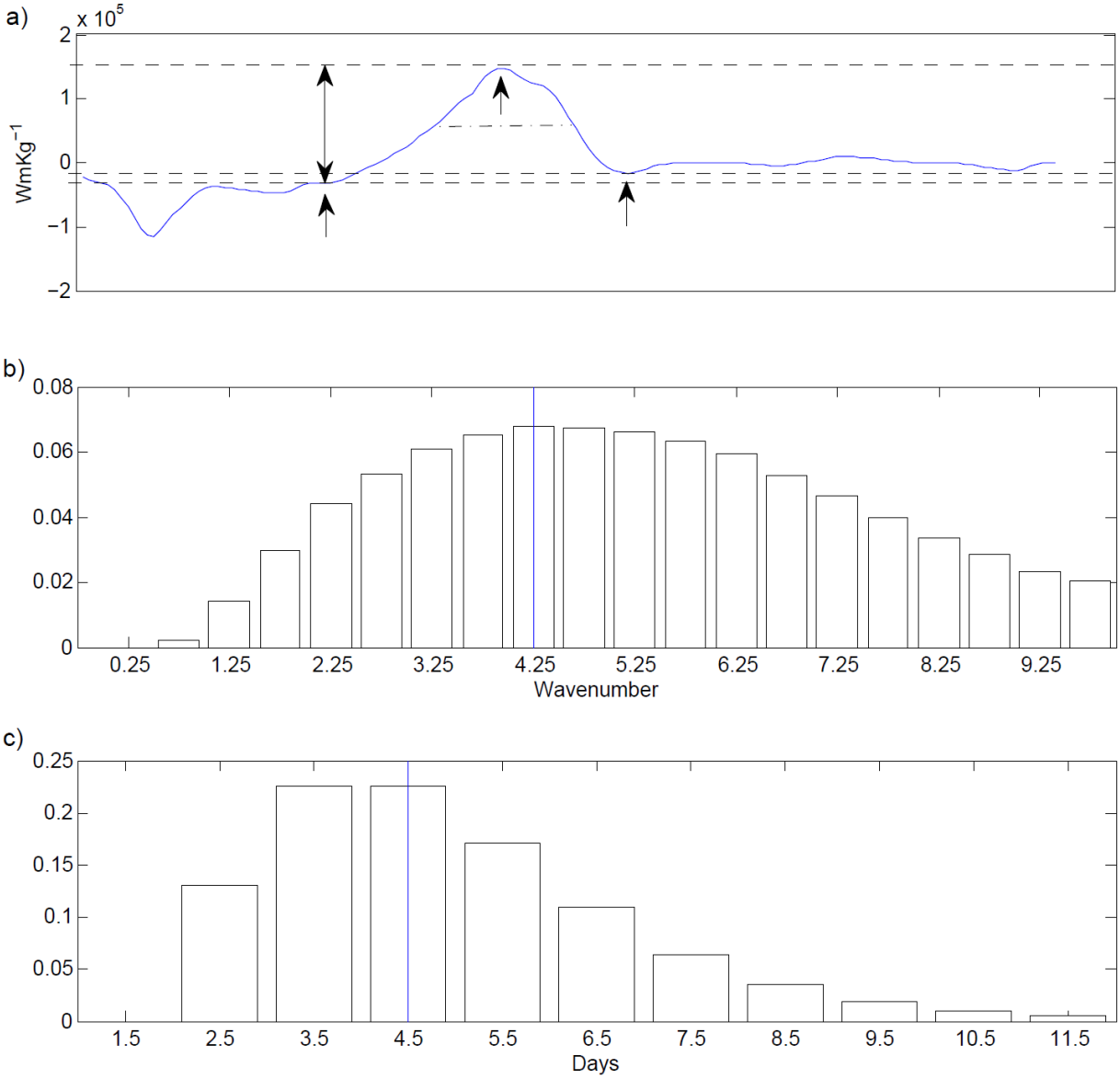

Figure 2: a) Schematic of how the full width/duration at half maximum of the v'H' signal is computed. The three arrows indicate the local maximum corresponding to an extreme event and the two local minima on either side. The double arrow indicates the height of the extreme event relative to the smaller of the two minima. The dash-dot line indicates the measured half-maximum width/duration (ω/τ). In this case, the peak is well defined relative to the local minima and the two minima are close to one another, meaning that the event passes all the aspect ratio tests (see text for details). The two bottom panels are PDFs of b) the wave number K and c) the full duration at half maximum T of extreme v'H' events. The latter are defined as events in the top 5 percentiles of the v'H' distribution. The data range is the same as in Figure 1. The vertical lines show the bins corresponding to the most likely values.

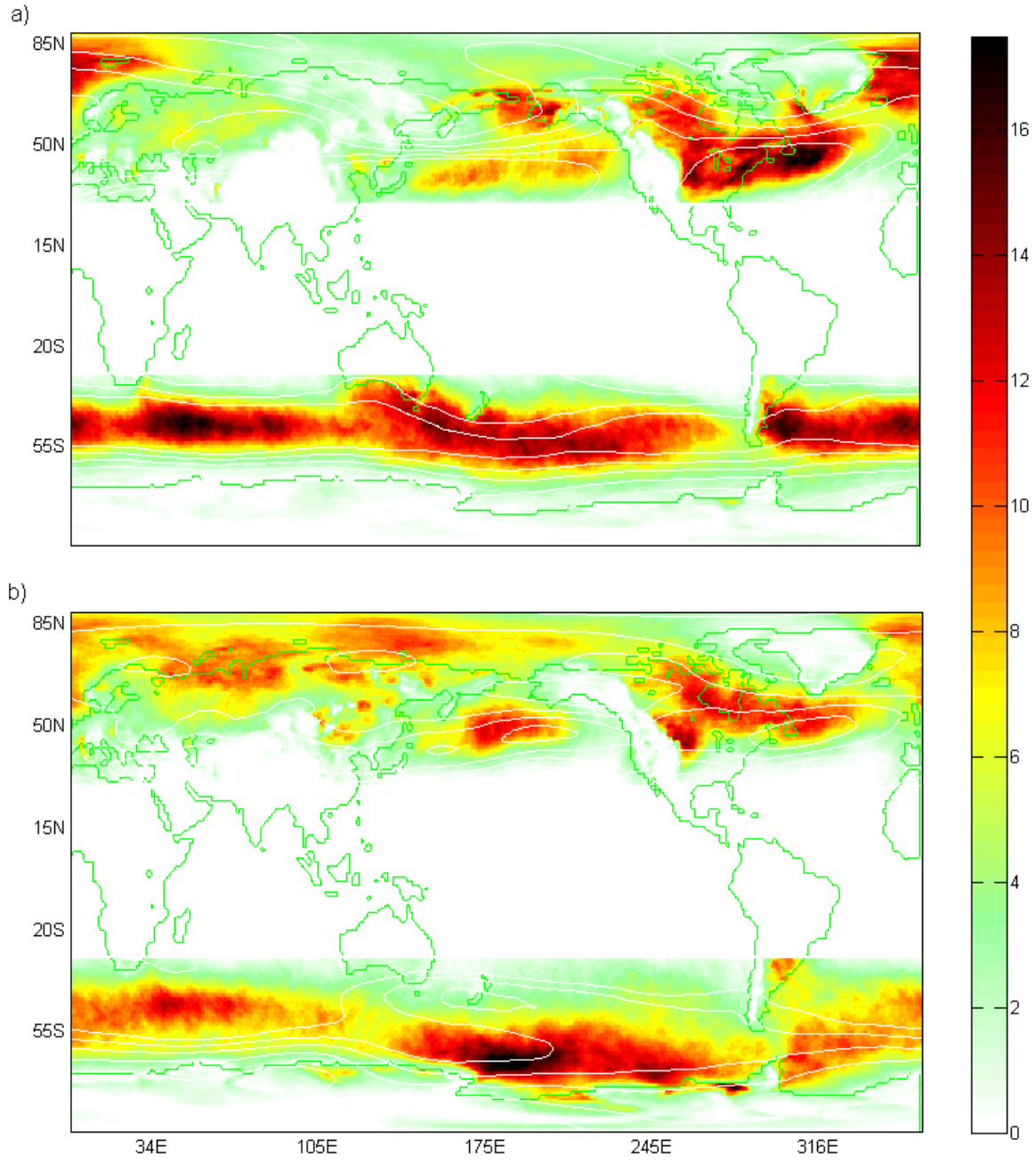

Figure 3: Map of v'H' events in the top 5 percentiles of the v'H' distribution for a) DJF and b) JJA. All twenty-four seasons (December 1993 – August 2005) are taken into consideration. The scale of the colour bar corresponds to the number of data points per season per 0.7° x 0.7° box. The calculation is not applied equatorward of 30° latitude. The white lines are regularly spaced 5 ms^{-1} contours of 300 mb time-averaged zonal winds. The contours range from 0 to 25 ms^{-1}, with positive wind speeds being eastbound.

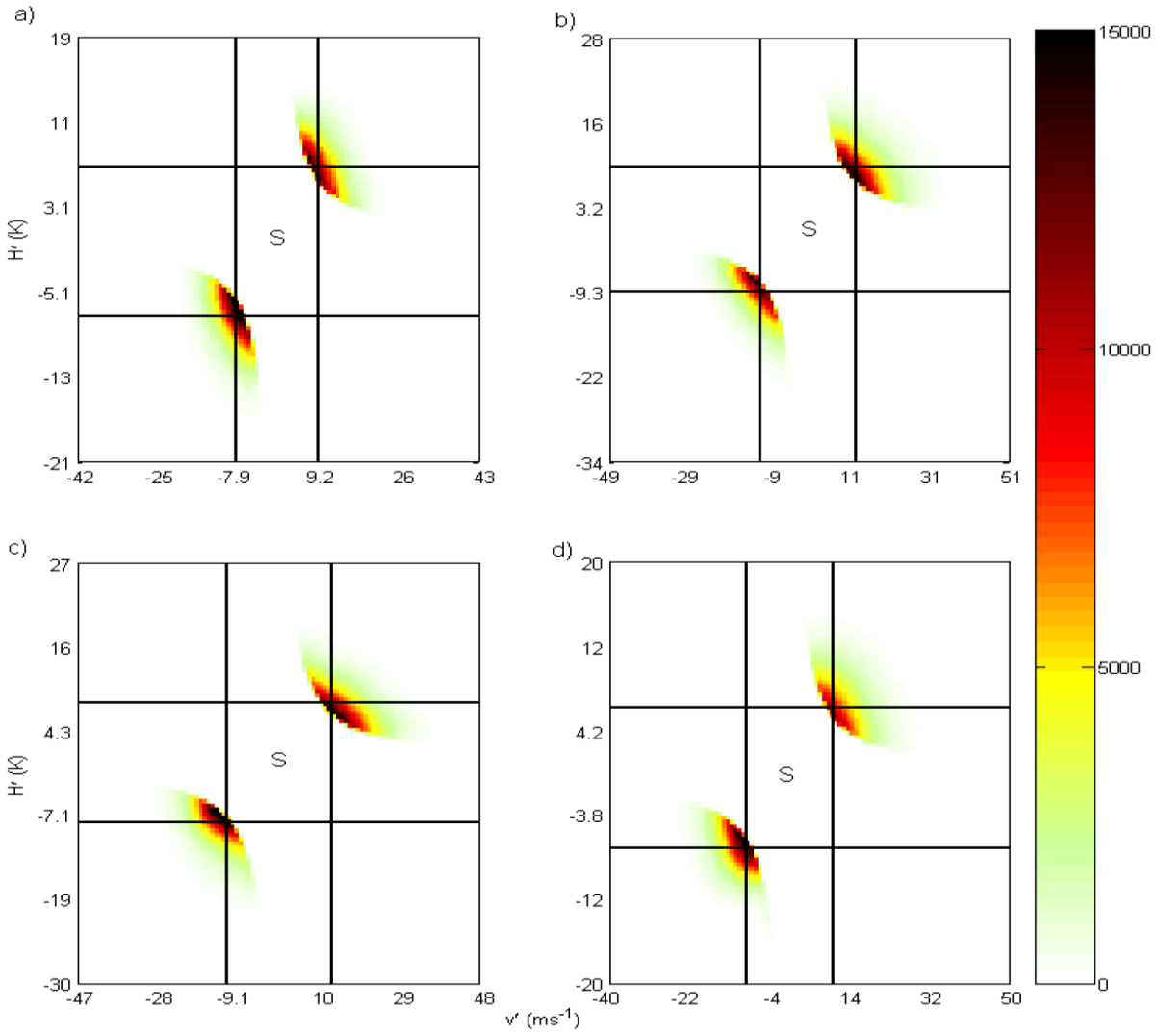

Figure 4: Colour map of v’ and H’ data points corresponding to the top 5 percentiles of v’H’ events for a) NH JJA, b) NH DJF, c) SH JJA and d) SH DJF. All twenty-four seasons (December 1993 – August 2005) are taken into consideration. The scale of the colour bar corresponds to the number of data points per discrete bin. The continuous lines correspond to the values of the 5th and 95th percentiles of the v’ and H’ distributions. The squares labelled S contain all extreme v’H’ occurrences where neither v’ nor H’ are in the top/ bottom five percentiles of their respective distributions.

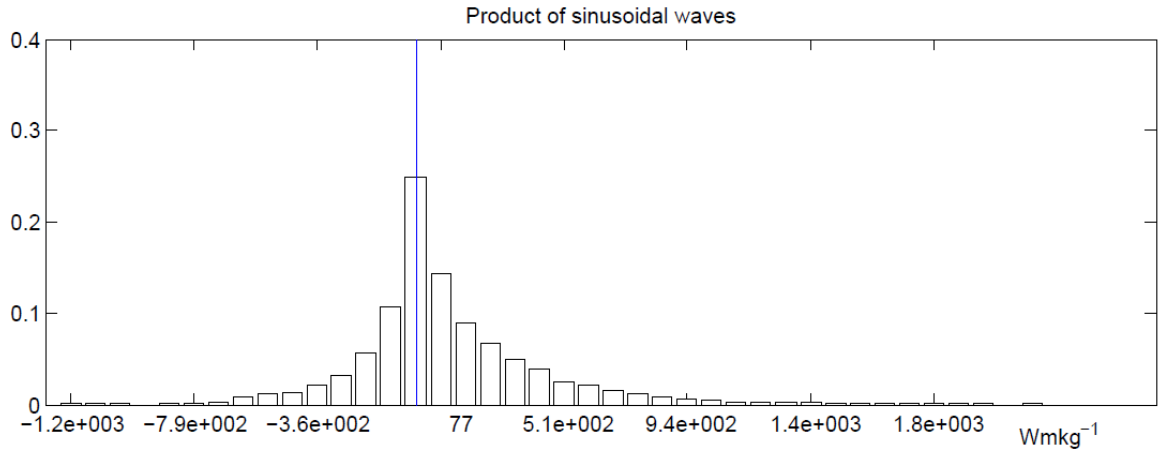

Figure 5: PDF resulting from the product of two linear sums of sinusoidal waves, taken as simple models for v' and H'. The following equations were adopted:

$$v' = \Sigma_i A_i \sin(ix + \varphi_i);\ H' = \Sigma_i B_i \sin(ix + \varphi_i + \Delta\varphi);$$

$$v'H' = \Sigma_i \Sigma_j A_i B_j \sin(ix + \varphi_i)\sin(jx + \varphi_j + \Delta\varphi).$$

Here i and j represent summation over a range of frequencies (corresponding to periods ranging from seasonal to daily scales), each with corresponding amplitudes A_i and B_j and random phases φ_i and φ_j. $\Delta\varphi$ is a fixed phase relationship between all v' and H' waves, here set to $\pi/10$ as an indicative near in-phase scenario. The distribution reproduces both the long positive tail and the near zero most likely value of the v'H' PDF seen in Figure 1c.

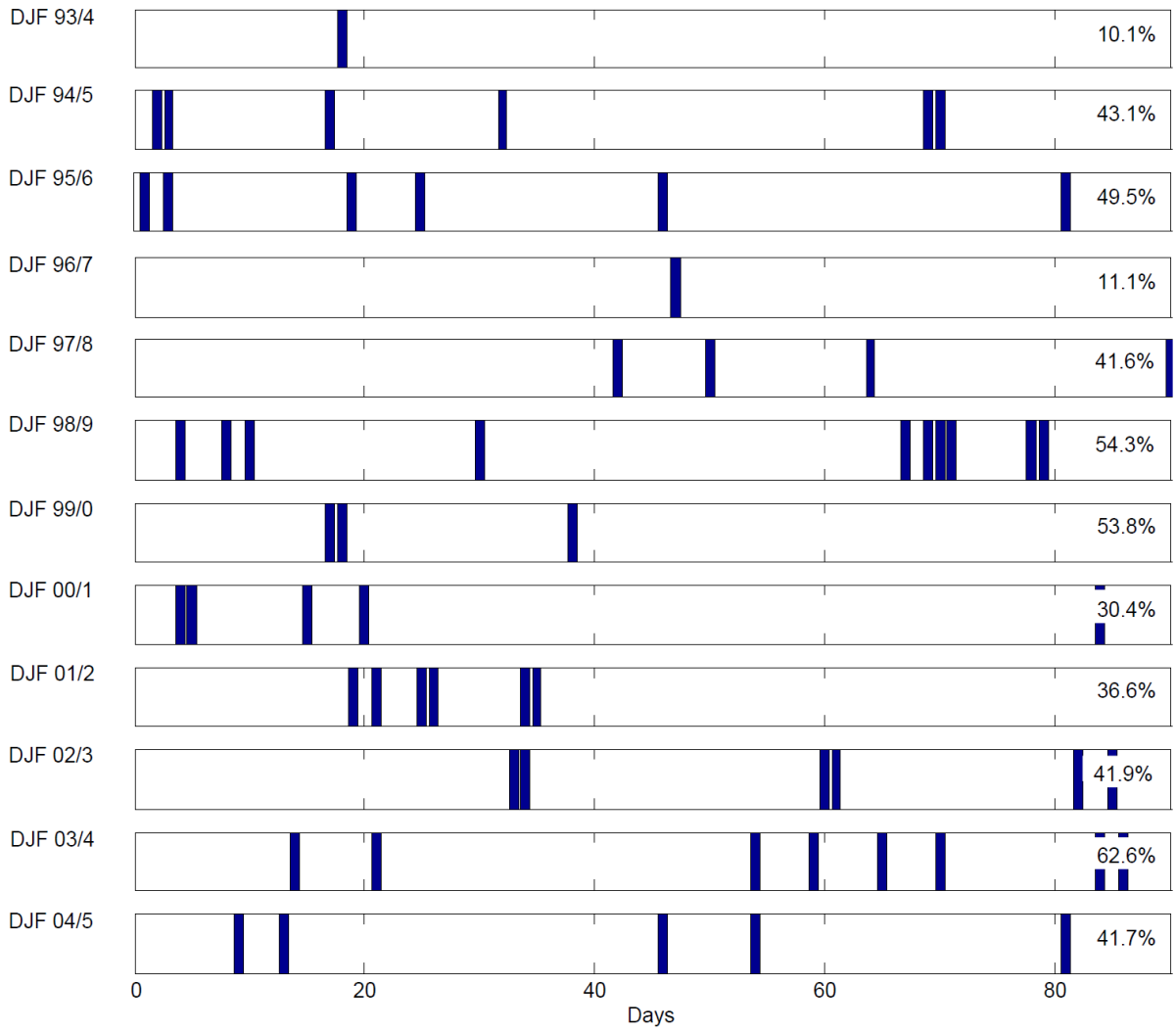

Figure 6: Bar plot of v'H' extreme events at 60°N 0°E. Extreme events are defined as events in the top 5 percentiles of the v'H' distribution for the 60°N latitude circle. The twelve panels correspond to DJF seasons from DJF 1993/4 to DJF 2004/5. Bars correspond to an extreme event occurring on a given day; the abscissa indicates the day of the season. The percentages in each panel indicate the contribution of the selected events to the net seasonal meridional transient eddy heat transport. See text for further details.